LUND UNIVERSITY

FACULTY OF SCIENCE

Goldilocks cooling: Demonstrating the quantum Mpemba effect in a two-level system

Lasse Ulbricht

Thesis submitted for the degree of Bachelor of Science
Project duration: 2 months, 15 ECTS

Supervisor: Peter Samuelsson
Co-supervisor: Daniel Holst

Department of Physics
Division of Mathematical Physics
June 2026

Abstract

This thesis investigates the quantum Mpemba effect, where an initially hotter system cools down faster than an initially colder one. This was demonstrated in a qubit system coupled to two environments. A thermal state is chosen as the initial state and then left to freely equilibrate. It was shown that the initial thermal state can be chosen in a way to accelerate the resulting relaxation process. The Liouvillian dynamics were analyzed and, by eliminating the contribution of the slowest decaying eigenmode (SDM) corresponding to accelerated relaxation dynamics, the effect was demonstrated. All states with vanishing SDM contributions were considered and found to belong to a plane in the Bloch sphere corresponding to a reduced state space. A thermal state could be shown to exist in this subspace, which is the Mpemba state that relaxes the fastest. The numerical relaxation dynamics were computed and the accelerated behavior of the Mpemba state verified. The fidelity of the Mpemba state also exhibits a steeper decay, consistent with the faster-decaying modes. The results were found to only strongly affect the solution in regions close to the steady state.

Acknowledgments

First and foremost I would like to thank Daniel and Peter for supervising and aiding with a lot of constructive discussions. I would especially like to thank Daniel, for coming up with the project and being always available for help and feedback. I would also like to thank the rest of the mesoscopic research group for a pleasant and smooth introduction to the world of research. On another note, thank you to Kyra and Lucas for keeping me company in the office, without you this project would have been a lot less fun. Thank you to all my friends for the support along the journey and the invaluable peer reviews. Lastly, thank you to my family, who were always there for me.

I acknowledge the use of generative AI tools for code debugging, plotting as well as minor paraphrasing.

Contents

List of abbreviations

- QME - quantum Mpemba effect
- ME - Mpemba effect
- SS - steady state
- SDM - slowest decaying mode

1 Introduction

Cooling is of fundamental importance in many modern applications. It is used in household appliances and computers but also necessary for superconducting quantum computers. Thermodynamically it is a well understood concept; systems that are hotter initially take longer to cool down and vice versa [1]. Statistical mechanics provides the tools to deal with the concept of temperature as a macroscopic variable based on statistical prediction of microscopic ensembles [2, 3]. However, there exist regimes on the nanoscale where the methods of classical thermodynamics are not useful anymore, since the variables pressure and volume do not describe the systems any longer [4]. Many interesting phenomena take place on this scale such as thermoelectricity and qubit energetics, requiring a quantum mechanical description [5]. The Quantum Mpemba effect (QME) named after the classical Mpemba effect (ME) is one such phenomenon.

The ME is the observation that, in some cases, a system initially at higher temperature can cool down faster than one initially at lower temperature [1]. Already Aristotle noted that, under certain circumstances, a hot liquid can cool faster than a cold one [6]. This effect was rediscovered in the 1960s by Erasto Mpemba, a middle school student at the time and popularized by D. G. Osborne who experimented on, and published, Mpemba's findings [7]. However, the ME is not a well established phenomenon, lacking reproducibility and physical explanations to a large extent [8, 9]. An analogous effect, with a different explanation is the QME; here, a quantum system in contact with an environment will also reach equilibrium and can do so at a faster rate under certain initial conditions, which can correspond to a higher initial temperature [10].

The timescale at which a system relaxes is important in many cases. For example, when studying the steady state (SS) it is impractical to have a long relaxation time, as the system will decohere and lose information [11]. An application of this could be quantum computation methods that are based on steady state encoding. Here, a method for finding an accelerated relaxation without energy cost could be useful [12]. Since there is a more rigorous mathematical framework for the QME, and due to its consequences for quantum thermodynamics, the focus of this thesis work will be on the quantum version of the ME in a two-level (qubit) system.

In the following a qubit system coupled to two environments will be investigated to demonstrate the QME as seen in Figure 1. To examine the qubit behavior the relaxation dynamics of a thermal state are computed using the Lindblad master equation. The properties of the slowest decaying mode (SDM) are investigated as they are intrinsically related to the relaxation timescale [13].

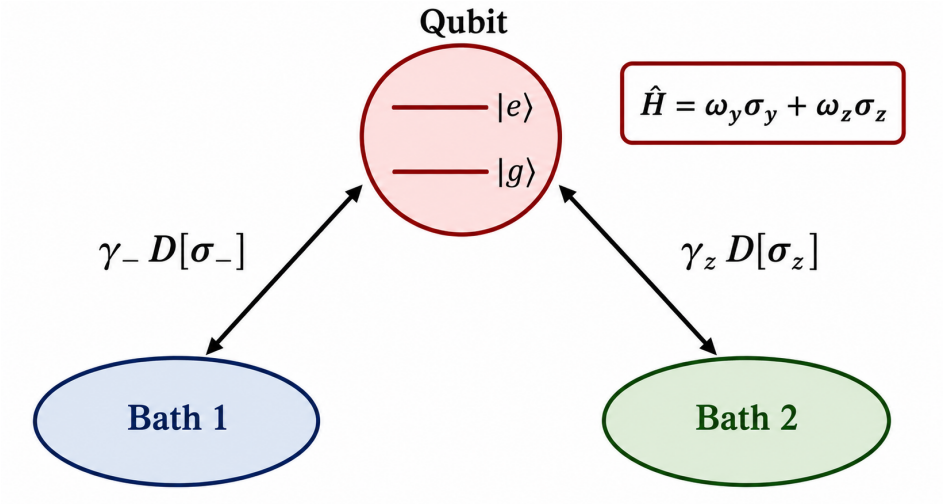

Figure 1: The setup: A qubit system is coupled to two baths and interacts with them via dissipative terms, modeled by the Lindblad equation. The qubit energy is described by the Hamiltonian $\hat{H}$, the coupling by $\gamma_{z/-}$ and the dissipation by $D[\sigma_{z/-}]$. (Figure created by ChatGPT, GPT-5.5 based on provided sketch.)

The system considered in this thesis is chosen to be a minimalistic system whilst still retaining the characteristics of a quantum system that can interact with an environment via dissipation and is prepared similarly to systems in other papers on the QME [14].

The system can be in either the excited state $|e\rangle$ or ground state $|g\rangle$, which corresponds to the eigenstates of the Hamiltonian. Given the system Hamiltonian, an initial state at a temperature T can be defined through a Gibbs state, where the probability of finding the qubit in the excited state, compared to the ground state, defines the temperature. The system is then brought into contact with the environment and can freely equilibrate. This is modeled via two thermal baths. In the case of a Hamiltonian with only a σ_z component, the σ_- bath acts as decay and the σ_z bath acts as dephasing. However, for a Hamiltonian with a non-zero σ_y component this simple decomposition of the effects no longer holds. The environmental couplings now in general drive the system into a SS that is not diagonal in the eigenbasis of $\hat{H}$.

The remainder of this thesis is organized as follows. In the next section the theoretical background will be presented, introducing the general framework of working with qubits, thermal states and the Lindblad equation. After that the methods used to investigate this effect along with the necessary calculations are presented. This is followed by both numerical and analytical results as well as a discussion of the obtained results. Lastly an outlook is presented on how the work on this topic could be continued.

2 Theoretical framework

To mathematically describe a system coupled to an environment, which is called an open quantum system, density matrices need to be used. The Lindblad master equation is a standard method for modeling the time evolution in open systems. Here, the Schrödinger equation is no longer sufficient in describing the dynamics, since in open quantum systems general state evolution is given by quantum channels (completely positive trace preserving linear maps) and not unitary operators [15].

2.1 Open quantum systems

Since not all quantum systems can be described by a singular state vector, a ket, there is the need for a more general description. Therefore the concept of a density operator, also known as a density matrix is introduced, which describes a quantum system as a statistical mixture of quantum states, thereby introducing classical randomness into the quantum system [16]. A general density matrix is defined as

$$\rho = \sum_i p_i |\psi_i\rangle\langle\psi_i|, \tag{1}$$

where the system is prepared in the state $|\psi_i\rangle$ with a probability p_i. Further it holds for all density matrices that they are Hermitian $\rho^\dagger = \rho$, positive semi-definite $\langle v|\rho|v\rangle \geq 0, \forall |v\rangle \in \mathcal{H}$ and have trace one $\mathrm{tr}(\rho) = 1$ [17]. Due to these conditions, density matrices can be diagonalized with real eigenvalues summing to one which means that the diagonal elements represent probabilities and correspond to the populations of the systems, while off-diagonal elements are referred to as coherences [16]. Furthermore, there is an important distinction between pure states and mixed states. Pure states need no classical probability description as they correpsond to a singular state

$$\rho = |\psi\rangle\langle\psi|, \tag{2}$$

with the important property that their purity is one, $\mathrm{tr}(\rho^2) = 1$. Mixed states lie in the convex hull of pure states, which leads back to the form of Equation 1. These have a purity of less than one, $\mathrm{tr}(\rho^2) < 1$.

An important property that is used to represent states is the function of an operator, given by

$$f(A) = \sum f(\lambda_i)|i\rangle\langle i|, \tag{3}$$

where λ_i are the eigenvalues of the operator A and $|i\rangle$ the corresponding eigenvectors.

2.2 The Bloch sphere

Qubits, meaning two level quantum systems, are the simplest quantum systems that are useful and thus well understood. A pure qubit state can be expressed as a superposition of its two states

$$|\psi\rangle = \alpha \begin{pmatrix} 0 \\ 1 \end{pmatrix} + \beta \begin{pmatrix} 1 \\ 0 \end{pmatrix} = \alpha|0\rangle + \beta|1\rangle. \tag{4}$$

Here $|0\rangle$ and $|1\rangle$ are the computational basis vectors in 2D. By expressing the complex numbers α and β in their polar representation, adding a global phase (which is allowed in quantum mechanics) and normalising, the qubit can be expressed as

$$|\psi\rangle = \cos\left(\frac{\Theta}{2}\right)|0\rangle + \sin\left(\frac{\Theta}{2}\right)e^{i\phi}|1\rangle. \tag{5}$$

This equation parametrizes a unit sphere, known as the Bloch sphere. It fully characterizes the qubit state space, meaning all qubits can be expressed as vectors in this sphere [15]. With this any qubit density matrix can be described by the following

$$\rho = \frac{1}{2}(\mathbb{I}_{2\times 2} + \bar{r} \cdot \bar{\sigma}), \tag{6}$$

where $\bar{\sigma} = (\sigma_x, \sigma_y, \sigma_z)$ are the Pauli matrices and $\bar{r} = (r_x, r_y, r_z)$ is the Bloch vector with $0 \leq ||\bar{r}|| \leq 1$, representing the position on the Bloch sphere [17]. Further this leads to a more intuitive description of pure and mixed states, where pure states are the ones lying on the sphere and mixed states are all those whose Bloch vector ends within the sphere.

2.3 The qubit Hamiltonian

The general Hamiltonian for a two level quantum system is given by

$$\hat{H} = \alpha \cdot \mathbb{I} + \bar{\omega} \cdot \bar{\sigma}, \tag{7}$$

where α, as well as the components of the vector $\bar{\omega} = (\omega_x, \omega_y, \omega_z)$ are real constants and $\bar{\sigma}$ is a vector of the Pauli matrices (here α and the components of $\bar{\omega}$ have units of energy so the ω_i are frequencies with $\hbar = 1$) [15]. Thus the general Hamiltonian is a linear combination of the identity matrix and the Pauli matrices. It is worth noting that Equation 7 is very similar to the general form of a density matrix as seen in Equation 6, which is more restricted due to the additional constraints on density matrices [16]. A much used property throughout this paper will be the norm of $\bar{\omega}$, $||\bar{\omega}|| = \Omega = \sqrt{\omega_x^2 + \omega_y^2 + \omega_z^2}$. Now the eigenvalues can be

generally written as

$$\lambda_{\pm} = \alpha \pm \Omega, \tag{8}$$

for any qubit Hamiltonian. The Hamiltonian used in this project will be

$$\hat{H} = \omega_y \sigma_y + \omega_z \sigma_z = \bar{\omega} \cdot \bar{\sigma}, \tag{9}$$

with $\bar{\omega} = (0, \omega_y, \omega_z)$ and no contribution from α since it does not affect the dynamics. This gives $\Omega = \sqrt{\omega_y^2 + \omega_z^2}$ and $\lambda_{\pm} = \pm\Omega$.

2.4 Thermal states and temperature in quantum systems

As the project is dealing with a temperature effect, a thermal quantum state has to be defined. The state of a quantum system in thermal equilibrium at temperature T is given by the quantum mechanical Gibbs state

$$\rho_{th} = \frac{e^{-\beta \hat{H}}}{Z}, \tag{10}$$

where $\beta = 1/T$ is the inverse temperature ($k_B = 1$ for the purpose of this thesis). $\hat{H}$ is the system's Hamiltonian and Z is the partition function which is given by $Z = \text{tr}\left(\exp\left(-\beta \hat{H}\right)\right)$ [5]. Thermal states, as any other states can be visualized in the Bloch sphere. The system Hamiltonian provides a natural orientation for the temperature axis in the Bloch sphere, given by $\bar{r} \propto \bar{\omega}$. Further, this state will be diagonal in the eigenbasis of the system Hamiltonian with real eigenvalues and of the form

$$\rho_{th} = \frac{1}{Z} \begin{pmatrix} e^{-\beta\Omega} & 0 \\ 0 & e^{\beta\Omega} \end{pmatrix}. \tag{11}$$

In this form the effect of temperature can be clearly seen. As the temperature goes to infinity, that is $\beta \to 0$ the state converges towards an equal mix of the ground and excited state. If the temperature tends to zero, $\beta \to \infty$ and the entire population will be in the ground state, ρ_{11}. If we instead work in the computational basis $|0\rangle$, $|1\rangle$ the thermal state is no longer diagonal but is given by:

$$\rho_{th} = \frac{1}{2} \begin{pmatrix} 1 - \beta_e \omega_z/\Omega & \beta_e i\omega_y/\Omega \\ -\beta_e i\omega_y/\Omega & 1 + \beta_e \omega_z/\Omega \end{pmatrix}, \tag{12}$$

where $\beta_e = \tanh(\beta\Omega)$. How the thermal state is calculated from Equation 10 is shown in Appendix A. This allows for a decomposition into Bloch vector form with

$$\bar{r} = \frac{\beta_e}{\Omega}(0, -\omega_y, -\omega_z). \tag{13}$$

From now on, β_e is referred to as the temperature factor since, given a value of Ω, there is a one-to-one correspondence between β_e and T. Investigating the temperature behavior it is found that $T \to 0 \implies \beta_e \to 1$ and $T \to \infty \implies \beta_e \to 0$. Further, since $||\bar{r}|| = \beta_e$ the temperature factor corresponds to the length of the Bloch vector of a given thermal state. It will always lie on the line spanned by the basis vectors of ρ_{th} and is defined on $\beta_e \in [0, 1)$. For vectors pointing the other direction in the same line, the populations would be inverted, meaning that the excited state could have a higher population than the ground state, corresponding to a negative temperature. This scenario will not be considered in this thesis. Further with the orientation of the temperature axis known via Equation 13 the angle between this new axis and the population axis (Z axis) can be defined. From basic trigonometry this angle is given by

$$\theta = \arctan\left(\frac{\omega_y}{\omega_z}\right). \tag{14}$$

The concept of temperature with respect to the chosen parameters in the Hamiltonian can be expressed in the Bloch sphere, which can be computationally implemented in Python using QuTiP, as can be seen in Figure 2.

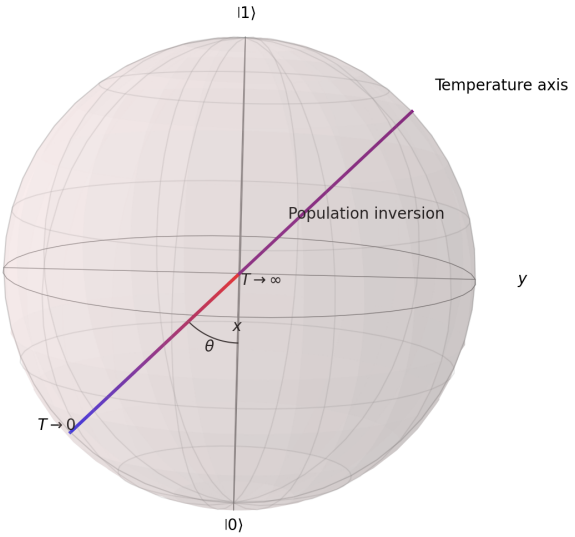

Figure 2: Bloch sphere with temperature axis indicated according to Hamiltonian. The density matrix corresponding to a thermal state has its Bloch vector lying on this axis with the length governed by β_e. The angle between the negative Z axis and the temperature axis is given by Equation 14.

Using this definition of temperature, a state at zero temperature will lie at the surface of the sphere and thus be a pure state and a state at infinite temperature will lie at the origin corresponding to a maximally mixed state.

2.5 The Lindblad master equation

Generally, a Markovian master equation describes the time evolution of a probabilistic system, which here is applied to open quantum systems [18]. A Markov process is a memoryless stochastic process. In Markovian dynamics the evolution of a state at time t only depends on t and not on the state at any previous time [15, 17]. The use of master equations of this form is justified by two main assumptions, the Born approximation and the Markov approximation. The Born approximation implies a weak system-environment interaction so that the baths can be assumed to be unaffected and only the system changes [16]. Further the reservoir correlation time should be much shorter than the system relaxation time. This means that the reservoir loses its memory of the system state quickly, relative to the pace at which the system evolves, so information is carried away from the system and does not flow back to it, which effectively erases memory in the dynamics and makes it Markovian [19]. This is known as the Markov approximation.

For open quantum systems the Lindblad master equation is the most general equation describing Markovian dynamics [15]. It is of the form

$$\frac{\partial \rho}{\partial t} = -i[\hat{H}, \rho] + \sum_k \gamma_k D[L_k], \tag{15}$$

where γ_k are the couplings to the different dissipative terms $D[L_k]$ which model the interaction with the environment. The γ_k set the timescale at which the system reaches the SS. The dissipative terms have the following form

$$D[L_k] = L_k \rho L_k^\dagger - \frac{1}{2}\{L_k^\dagger L_k, \rho\}. \tag{16}$$

The L_k are the Lindblad operators, which are a set of operators chosen to represent the coupling of system to environment and $\{\alpha, \beta\} = \alpha\beta + \beta\alpha$ is the anti-commutator [17]. The master equation can also be expressed in terms of a Liouvillian superoperator, that is an operator that acts on operators:

$$\frac{\partial \rho}{\partial t} = \mathcal{L}(\rho(t)), \tag{17}$$

which is a differential equation that is solved by

$$\rho(t) = e^{\mathcal{L}t}\rho(0), \tag{18}$$

when $\mathcal{L}$ is time-independent. Since the Liouvillian is an operator that acts on matrices, it can be difficult to represent. To simplify this the Choi-Jamiolkowski isomorphism can be applied, vectorizing the density matrices by rows where $\{|i\rangle\}$ are the computational basis vectors

$$|i\rangle\langle j| \to |i\rangle \otimes |j\rangle \implies \rho = \sum_{i,j} \rho_{i,j}|i\rangle\langle j| \to \text{vec}(\rho) = \sum_{i,j} \rho_{i,j}|i\rangle \otimes |j\rangle. \tag{19}$$

This will turn the elements of a generic qubit density matrix (2x2) into a column vector $\rho = (\rho_{00}, \rho_{01}, \rho_{10}, \rho_{11})^T$. Further the vectorization identity $\text{vec}(ABC) = (A \otimes C^T)\,\text{vec}(B)$ can be used to find the Liouvillian in matrix form by correctly applying identity matrices [18]

$$\mathcal{L} = -i(\hat{H} \otimes \mathbb{I} - \mathbb{I} \otimes \hat{H}^T) + \sum_k \gamma_k [L_k \otimes L_k^* - \frac{1}{2}\mathbb{I} \otimes (L_k^\dagger L_k)^T - \frac{1}{2} L_k^\dagger L_k \otimes \mathbb{I}]. \tag{20}$$

Using this, the equations of motion can be solved using the spectral decomposition of $\mathcal{L}$, which will have left and right eigenvectors due to not being hermitian anymore

$$\mathcal{L}|r_k\rangle = \lambda_k |r_k\rangle \tag{21}$$

$$\langle l_k|\mathcal{L} = \langle l_k|\lambda_k \implies \mathcal{L}^\dagger |l_k\rangle = \lambda_k^* |l_k\rangle. \tag{22}$$

The eigenvectors can be determined by diagonalization, and are normalized by $\sqrt{\langle l_k|r_k\rangle}$. Importantly, the left eigenstates, cannot be found by the hermitian conjugate of the right eigenstates anymore but have to be found by diagonalizing $\mathcal{L}^\dagger$ instead, as seen in Equation 22. After normalization the left and right eigenvectors will form a biorthonormal basis $\langle l_i|r_j\rangle = \delta_{ij}$, which allows us to use them for a spectral decomposition of $\mathcal{L}$ [20]

$$\mathcal{L}(t) = e^{\mathcal{L}t} = \sum_{k=1}^{d^2} e^{\lambda_k t} |r_k\rangle\langle l_k|, \tag{23}$$

where d is the dimensionality of the system ($d = 2$). Further it can be shown that any time-independent Liouvillian will always have at least one zero eigenvalue corresponding to the existence of a steady state. The left eigenvector of the zero eigenvalue will be identity due to trace preservation [18] and shall always be the first indexed eigenvalue with corresponding

eigenvectors. Thus we can split up the Liouvillian

$$\mathcal{L}(t) = e^{\mathcal{L}t} = |r_1\rangle\langle\mathbb{I}| + \sum_{k=2}^{d^2} e^{\lambda_k t}|r_k\rangle\langle l_k|, \tag{24}$$

which, when acting on an arbitrary initial (vectorized) density matrix $|\rho(0)\rangle$, results in

$$\mathcal{L}(t)|\rho(0)\rangle = |r_1\rangle + \sum_{k=2}^{d^2} c_k e^{\lambda_k t}|r_k\rangle, \tag{25}$$

where $c_k = \langle l_k|\rho(0)\rangle$ and $\langle\mathbb{I}|\rho(0)\rangle = 1$ due to the trace one property of density matrices. Furthermore, as the dynamics are dissipative and thus should die out over time, the eigenvalues of the Liouvillian have a negative real part $0 \geq Re(\lambda_k), \forall k$. Therefore the exponentials will tend to zero in the long time limit $t \to \infty \implies e^{\lambda_k t} \to 0$, making the determination of r_1 the steady state solution of the system $|r_1\rangle = |\rho_{ss}\rangle$ [16].

2.6 Fidelity

To quantify the difference between two quantum states, the wavefunction overlap is commonly used as it relates to distance. However, when working with density matrices many different quantifiers are used. One of the most common ones is the fidelity

$$F(\rho, \sigma) = \left\|\sqrt{\rho}\sqrt{\sigma}\right\|_1^2 = \left(\mathrm{tr}\left(\sqrt{\sqrt{\sigma}\rho\sqrt{\sigma}}\right)\right)^2, \tag{26}$$

where σ and ρ are density matrices. Since $F(\rho, \rho) = 1$ the difference between 2 states is defined between 1 and 0, with 0 meaning the states are orthogonal and 1 meaning they are the same [15]. To make this compatible with the more common definition of distances, where 0 corresponds to the shortest distance the measure $1 - F(\rho, \sigma)$ is often used, known as the infidelity. It is worth noting that neither the infidelity nor the fidelity are actually distance measures since they lack a triangle inequality but for the purpose of showing how similar two states are they are sufficient and commonly used [15].

3 Method

In the following the method for achieving the QME is presented. For that, as previously mentioned the contribution of the SDM should be eliminated corresponding to $\langle SDM|\rho(0)\rangle = 0$. Here $\langle SDM|$ is the left eigenvector of the SDM and $|\rho(0)\rangle$ is the initial state. In the rest of this thesis the notation $|\rho\rangle = \text{vec}(\rho)$ will be used for vectorized states and eigenvectors as introduced in Section 2.5.

3.1 Removal of slowest decaying mode

To achieve the QME multiple methods can be used [1]. One of the most common methods that will also be employed here is the minimization of the SDM in the Liouvillian relaxation dynamics [14].

As seen in Equation 23 the dynamics can be described by diagonalizing the superoperator and expressing the time evolution as a spectral decomposition. The characteristic relaxation time, also called decay time, is now governed by the eigenvalues, which have a negative real part by construction. Since the ordering of eigenvalues does not matter they will be ordered by descending real parts $0 > Re(\lambda_2) > Re(\lambda_3) > Re(\lambda_4)$. The exponential time evolution leads to defining the decay time as $\tau = |\frac{1}{Re(\lambda_i)}|$ [14] leading to the condition that the relaxation will be governed by the least negative eigenvalue which will be the SDM, since it has the longest decay time. With this, the corresponding eigenvalues and eigenvectors are relabeled, $\lambda_2 = \lambda_{SDM}$, $\langle l_2| = \langle SDM|$. Thus by eliminating the contribution of the SDM the overall dynamics can be accelerated to reach the SS faster. This is of course under the constraint that the eigenvalues are distinct and that $\mathcal{L}$ is diagonalizeable. How drastic the effect will be depends on how much the real parts of the eigenvalues differ from one another.

From Equation 25 it can be seen that minimizing the SDM can be achieved by requiring $c_2 = \langle SDM|\rho(0)\rangle = 0$. Keeping the environment, which defines the SDM, fixed, this can be accomplished by changing the prepared initial state in such a way that it is orthogonal to the SDM.

3.2 Intersection method with Bloch sphere

The condition $c_2 = 0$ can be visualized in the Bloch sphere. Since any initial state (thermal or not) will lie in the Bloch sphere, states that are orthogonal to $\langle SDM|$ can be determined by parametrizing an arbitrary qubit state. This is done by using Equation 6, from which it can be seen that any state can be parametrized by (r_x, r_y, r_z). Thus the most general

equation for the intersection would be

$$\langle SDM|\rho_i\rangle = \langle SDM|\,\mathrm{vec}(\frac{1}{2}(\mathbb{I} + \bar{r}\cdot\bar{\sigma})) = 0. \tag{27}$$

Since this is an equation with two free parameters the most general solution is a plane, which will be the state space orthogonal to the SDM and thereby related to accelerated relaxation dynamics.

The relation of thermal states to this plane needs to be investigated, since the temperature is the parameter of interest. The state closest to this plane should be determined with respect to temperature (β_e). A plane is given in its point normal form as

$$\bar{n}\cdot\bar{r} = -d, \tag{28}$$

where $\bar{n}$ is the normal vector of the plane, $\bar{r}$ is the position vector of any point in the plane and d is a scalar that fixes the distance and orientation relative to the origin. With respect to this plane, the object of interest is

$$\min_{0\leq\beta_e\leq 1}(\bar{n}\cdot\bar{r}_{th} = -d). \tag{29}$$

The temperature factor β_e that minimizes Equation 29 will correspond to an optimal temperature. This temperature, corresponding to a minimization of the SDM should now exhibit Mpemba behavior since for all other values the larger contribution of the SDM will slow down the relaxation towards the steady state.

3.3 Finding the slowest decaying mode with the Lindblad formalism

With the Hamiltonian and two dissipators as given in Figure 1 the Lindblad equation for this system becomes

$$\mathcal{L}\rho = \frac{\partial\rho}{\partial t} = -i[\hat{H},\rho] + \gamma_- D[\sigma_-] + \gamma_z D[\sigma_z], \tag{30}$$

where the Liouvillian superoperator in vectorized form can be calculated according to Equation 20. To simplify calculations the coupling parameters will be the same $\gamma = \gamma_z = \gamma_-$. In

this form the Liouvillian becomes

$$\mathcal{L} = \begin{pmatrix} -\gamma & -\omega_y & -\omega_y & 0 \\ \omega_y & -\frac{5\gamma}{2} - 2i\omega_z & 0 & -\omega_y \\ \omega_y & 0 & -\frac{5\gamma}{2} + 2i\omega_z & -\omega_y \\ \gamma & \omega_y & \omega_y & 0 \end{pmatrix}. \tag{31}$$

This can now be used to find the left eigenvectors as well as the eigenvalues according to Equation 22. The eigenvalues are given by $\lambda_1 = 0$ as well as half the roots of the cubic

$$2\lambda_{2,3,4} \implies (80\omega_y^2\gamma + 32\omega_z^2\gamma + 50\gamma^3 + (16\omega_y^2 + 16\omega_z^2 + 45\gamma^2)\lambda + 12\gamma\lambda^2 + \lambda^3) = 0. \tag{32}$$

From this the eigenvalues can be found using Cardano's formula as

$$2\lambda_2 = -4\gamma + \sqrt[3]{-\frac{q}{2} + \sqrt{\Delta}} + \sqrt[3]{-\frac{q}{2} - \sqrt{\Delta}}, \tag{33}$$

as well as

$$2\lambda_{3,4} = -4\gamma + (\frac{-1 \pm \sqrt{3}i}{2})\sqrt[3]{-\frac{q}{2} + \sqrt{\Delta}} + (\frac{-1 \mp \sqrt{3}i}{2})\sqrt[3]{-\frac{q}{2} - \sqrt{\Delta}}, \tag{34}$$

with the discriminant

$$\Delta = \left(\frac{q}{2}\right)^2 + \left(\frac{p}{3}\right)^3. \tag{35}$$

The values for q and p are given by $q = -2\gamma(\gamma^2 - 8\omega_y^2 + 16\omega_z^2)$ and $p = -3\gamma^2 + 16(\omega_y^2 + \omega_z^2)$. If $\Delta > 0$ there is one real eigenvalue and a complex conjugate pair. Using this, a condition can be derived for λ_2 being the SDM, namely that the first root of the depressed cubic w_0 is greater than 0

$$w_0 = \sqrt[3]{-\frac{q}{2} + \sqrt{\Delta}} + \sqrt[3]{-\frac{q}{2} - \sqrt{\Delta}} > 0, \tag{36}$$

The derivation and the actual expression as well as the use of Cardano's formula to compute the eigenvalues is found in Appendix B.

The eigenvalue in Equation 33 can then be used to find $\langle SDM|$. All other right and left eigenvectors can also be found in a similar fashion but since they only matter for computationally simulating the relaxation dynamics they will not be presented here. However for convenience the effective eigenvalue used will be $\lambda_S = 2\lambda_2$ and $\Lambda = 5\gamma + \lambda_S$. Then the left eigenvector of the slowest decaying mode is given by

$$\langle SDM| = \left(\frac{\lambda_S\left(\Lambda^2 + 16\omega_z^2\right)}{8\omega_y^2\Lambda} + 1, \quad -\frac{\lambda_S(\Lambda - 4i\omega_z)}{4\omega_y\Lambda}, \quad -\frac{\lambda_S(\Lambda + 4i\omega_z)}{4\omega_y\Lambda}, \quad 1\right). \tag{37}$$

Since the left eigenvectors just map the initial state to a coefficient they do not need to have either trace one or trace zero as can be seen here. The eigenvector is left unnormalized, as it does not affect the set of states to which it is orthogonal. This eigenvector together with the vectorized form of an arbitrary qubit density matrix

$$|\rho_i\rangle = \frac{1}{2}(1 + r_z, r_x - ir_y, r_x + ir_y, 1 - r_z), \tag{38}$$

gives the equation of a plane in $\bar{r} = (r_x, r_y, r_z)$ as explained above. The plane is then described by

$$\bar{n} = (-4\lambda_S, \quad \frac{16\lambda_S\omega_z}{\Lambda}, \quad \frac{\lambda_S\left(\Lambda^2 + 16\omega_z^2\right)}{\omega_y\Lambda}), \tag{39}$$

and

$$d = \frac{\lambda_S\left(\Lambda^2 + 16\omega_z^2\right)}{\omega_y\Lambda} + 16\omega_y. \tag{40}$$

With this, the value of β_e can be found for which the thermal state lies in the plane, implying some temperature at which the SDM is eliminated. This means, the Bloch vector for the thermal state, (in the computational basis) given by $\bar{r}_{th} = (\beta_e/\Omega)(0, -\omega_y, -\omega_z)$, can be used to find the minimal β_e

$$\bar{n} \cdot \bar{r}_{th} = -d \implies \beta_e^{QME} = \frac{\Omega\left(16\omega_y^2\Lambda + \lambda_S\left(\Lambda^2 + 16\omega_z^2\right)\right)}{\lambda_S\omega_z\left(\Lambda^2 + 16\Omega^2\right)}, \tag{41}$$

from which

$$\beta_e^{QME} = \tanh\left(\frac{\Omega}{T}\right) \implies T_{QME} = \frac{\Omega}{\operatorname{arctanh}(\beta_e^{QME})}. \tag{42}$$

This means that the thermal state corresponding to this β_e^{QME} will lie in the plane, if it has a solution with physical meaning, which can be easily visualized in the Bloch sphere. Another useful property of Equation 42 is that it reduces to one when the ω_y contribution disappears

$$\omega_y \to 0 \implies \beta_e^{QME} \to \frac{\omega_z(\lambda_S(\Lambda^2 + 16\omega_z^2)}{\lambda_S\omega_z(\Lambda^2 + 16\omega_z^2)} = 1. \tag{43}$$

Since a temperature factor of one corresponds to zero temperature, $T = 0$, there is no more QME in this case since the fastest relaxing state is already in the ground state.

3.4 Determining the parameters ω_y,ω_z and γ

To apply the formalism described in the previous section, the parameters ω_y, ω_z and γ first have to be determined. To work out the dependencies, γ is left as a parameter and then ω_y, ω_z are parametrized accordingly: $\tilde{\omega}_y = \omega_y/\gamma$ and $\tilde{\omega}_z = \omega_z/\gamma$. For the model to work it

is important that the condition in Equation 36 is fulfilled. Numerically, this can be seen by plotting the eigenvalues for some parameter region and then choosing suitable values.

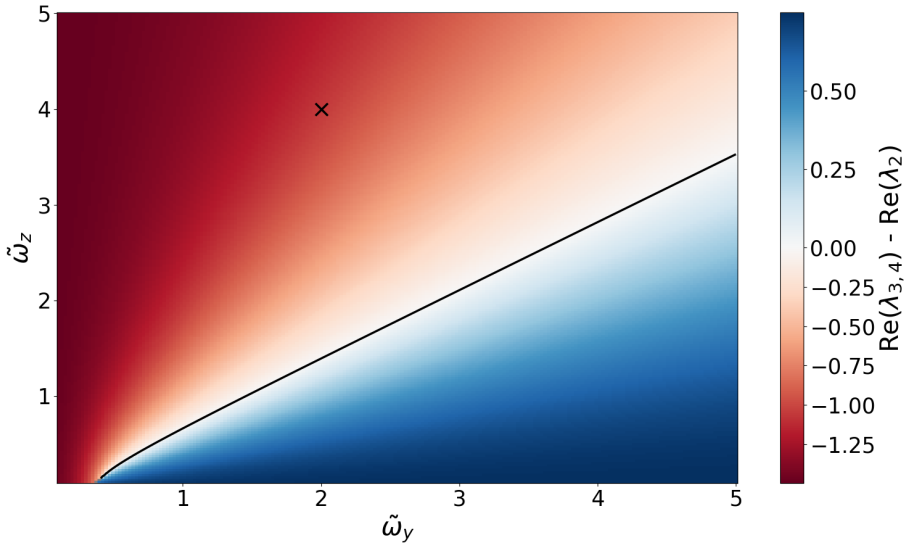

Figure 3: Contour plot of eigenvalue behavior. The black line corresponds to the bound given by Equation 36. Above the line $w_0 > 0$, which corresponds to a negative eigenvalue difference as expected. The X indicates the chosen parameters for further steps.

As can be seen in Figure 3 there is quite a large region accessible, all values above the line could be used. In order to have clearly distinct eigenvalues, which in turn leads to more distinct differences in the relaxation behavior, a large negative value of $Re(\lambda_{3,4}) - Re(\lambda_2)$ is favorable. However another constraint is given by the temperature factor. To have a sizable effect and show faster relaxation compared to colder initial temperatures the chosen state should not lie close to the zero temperature limit $\beta_e \to 1$. Based on Equation 41 the behavior of β_e^{QME}, from now on also referred to as Mpemba temperature (even though it is not strictly speaking a temperature but corresponds to one), can be visualized in a similar fashion to Figure 3. Figure 4 implies that optimally the parameters should be chosen in a way that the temperature factor lies on the white line. Further, a crude estimation of the parameters $\omega_y, \omega_z, \gamma$ can be made to highlight how an approach such as this one could translate into experiment. The frequencies $\omega_{y/z}$ can be chosen to be Rabi-frequencies corresponding to lasers as was done in [13], for example $\omega_y = 2\pi \times 20\,\mathrm{kHz}$ and $\omega_z = 2\pi \times 40\,\mathrm{kHz}$. Further γ has to be determined since it sets the timescale, which can be chosen to $\gamma = 10\,\mathrm{kHz}$ such that with time unit $\gamma t = 1$ the corresponding time is $100\,\mu\mathrm{s}$, which is a reasonable timescale for experiments to be made.

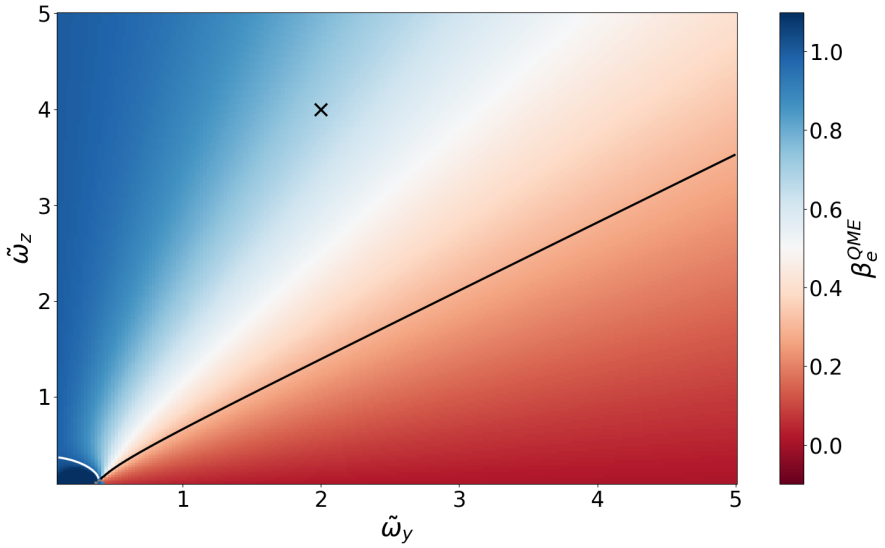

Figure 4: Contour plot of the Mpemba temperature. Red corresponds to higher temperatures and blue corresponds to colder temperatures. The white and black lines enclose regions that are not viable due to different constraints, all values above these lines are viable. Black: Eigenvalue constraint as seen in Figure 3. White: Constraint on the temperature scale $0 \leq |\beta_e| \leq 1$. The gray points could not be associated with a β_e^{QME} due to constraints regarding dividing by zero. The X indicates the chosen parameters for further steps.

4 Results

The presented results are based on the general equations derived in the previous section as well as the chosen parameters $\tilde{\omega}_y = 2, \quad \tilde{\omega}_z = 4$ unless otherwise stated. The resulting dynamics are presented as well as visualizations in the Bloch sphere and the time evolution of the fidelity.

4.1 Visualization in the Bloch sphere

The temperature factor that eliminates the SDM can be determined by Equation 41 to be $\beta_e^{QME} = 0.694$. With the state corresponding to this temperature factor, from now on called the Mpemba state, the elimination of the SDM can be visualized. Further a hotter and a colder state are introduced, to put the properties of the Mpemba state in relation to other thermal states. For this the states with $\beta_e = \beta_e^{QME} \pm 0.2$ were arbitrarily chosen, resulting in $\beta_e^{hot} = 0.494$ and $\beta_e^{cold} = 0.894$. These are the values of β_e for all following plots concerning colder and hotter states.

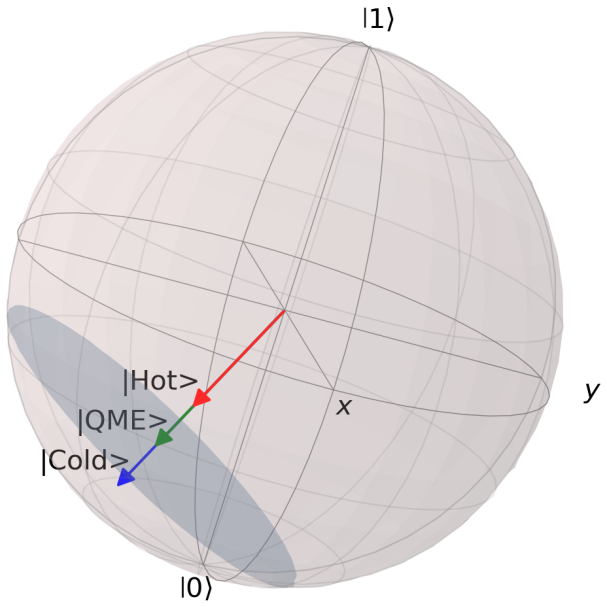

Figure 5: Bloch vectors of different thermal states in the Bloch sphere. The plane, corresponding to a vanishing SDM, $\langle SDM|\rho_i\rangle = 0$, is marked in grey. The red state corresponds to β_e^{hot} and the blue state to β_e^{cold}. The Mpemba state (green) with β_e^{QME} lies in the plane.

In Figure 5 it can be clearly seen that the plane corresponding to accelerated relaxation indeed includes a thermal state for some temperature β_e^{QME}. All other thermal states will have a different β_e and thus not lie in the plane, making the Mpemba state the only thermal

state with accelerated relaxation dynamics. Further, this plane, which describes a reduced state space, includes a lot more states that are not thermal.

4.2 Time evolution of the system

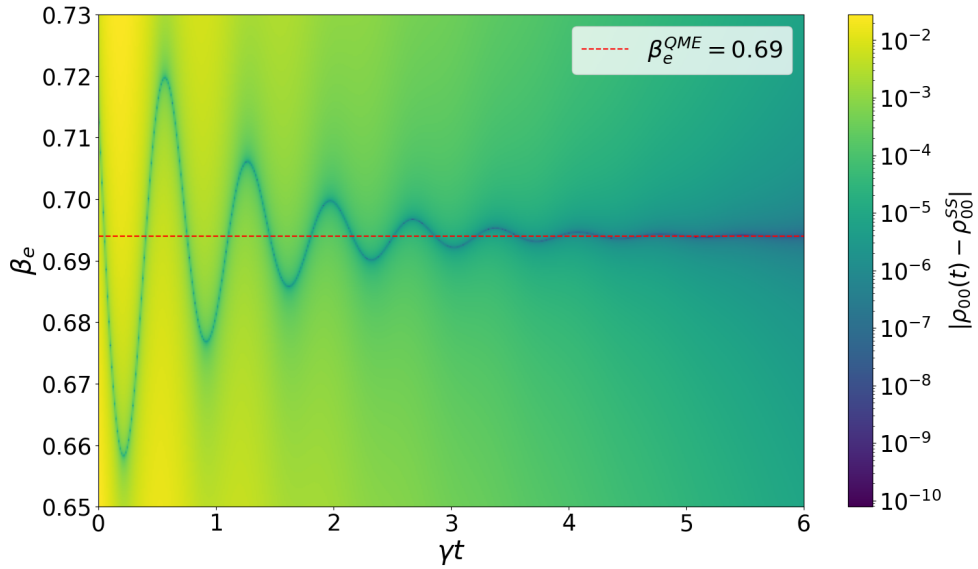

(a) Relaxation behavior of populations. The other populations ρ_{11} are easily found due to the trace condition, ($\rho_{11} = 1 - \rho_{00}$).

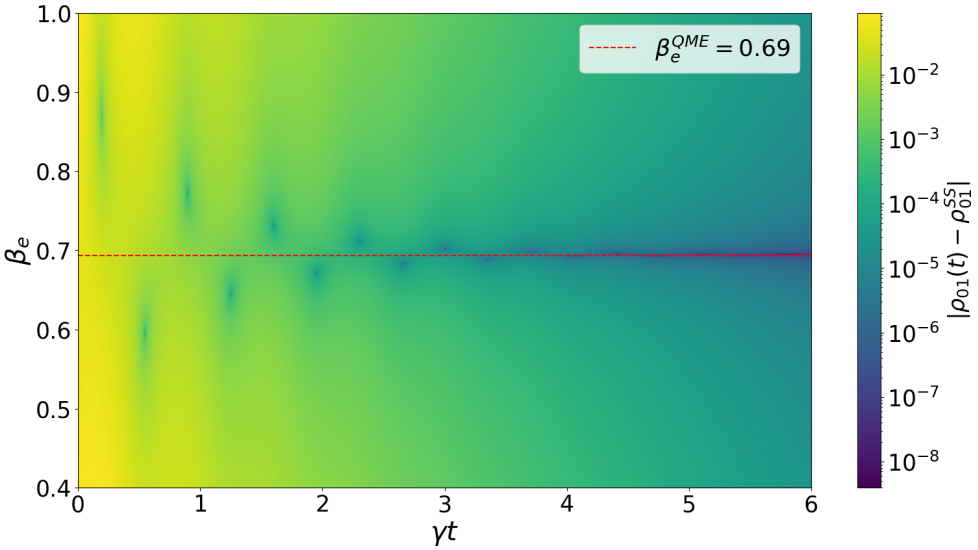

(b) Relaxation behavior of the coherences, which is the same for both due to the absolute value and hermiticity of density matrices $|\rho_{01}| = |\rho_{10}|$

Figure 6: Contour plot of the relaxation towards SS of different initial temperatures modeled as the absolute difference between a matrix element at some γt and the corresponding SS matrix element. Here, populations and coherences refer to matrix elements in the computational basis. The difference is presented on a log scale to highlight the oscillations, yellow corresponds to a state further away from the SS and blue to a state very close to the SS. The Mpemba temperature is highlighted by the red dashed line.

Seeing as the relaxation dynamics should differ greatly between the Mpemba state and any other state the time evolution can be investigated using the full dynamics described by Equation 24. In Figure 6 it can be seen that the temperature factor of the state that is closest to the SS oscillates in time but converges to the Mpemba state as indicated by the red line. This is also the case for the coherences where the oscillations follow a different pattern but still converge towards the Mpemba state. However, it should be noted that this convergence happens at $\gamma t > 3$ where the total differences from the SS value are already very small for all states initial states $|\rho_{00}(t) - \rho_{00}^{SS}| < 10^{-4}$.

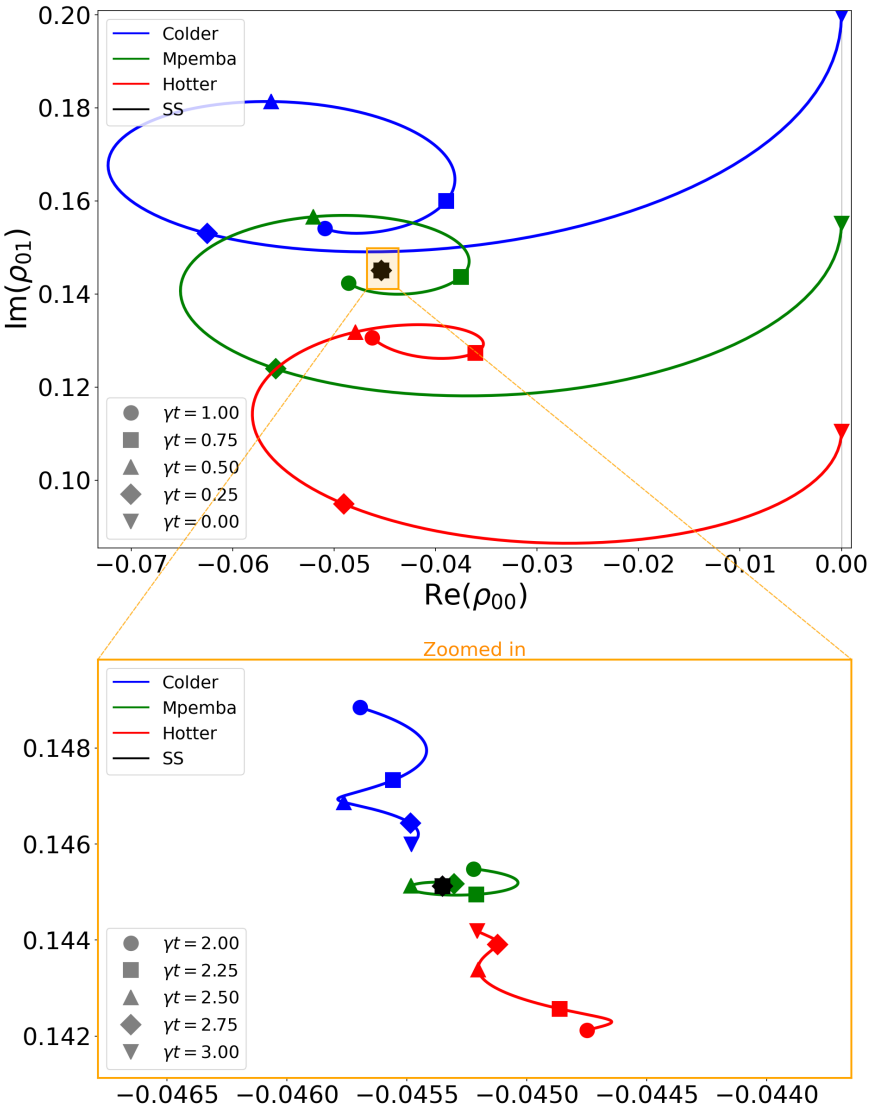

Figure 7: Relaxation of the coherences of different initial states in the complex plane. The time evolution is indicated by different timestamps along the trajectory, and a zoomed in version is presented for the time evolution from $\gamma t = 2$ to $\gamma t = 3$. The full trajectories are truncated for readability. The SS is indicated by the black dot, as it does not move with time. The time step $\gamma t = 1$ to $\gamma t = 2$ was omitted here, as it is more insightful to look at the next step. All timesteps can be found in Appendix C.

By looking at the relaxation in Figure 7 it can be seen that the Mpemba state does indeed relax faster than both the hotter and the colder state as expected. In Figure 7 the relaxation behavior is similar between all states, while at a later time, in the zoomed in picture, the hotter and colder state oscillate towards the SS while the Mpemba state is already oscillating very closely around the SS. The scale at which the oscillations differ is very small, which is similar to the behavior seen in Figure 6. However, both Figure 6 and Figure 7 only present either the coherences or populations in the computational basis. Since the thermal states are not diagonal in this basis, the whole density matrix has to be considered and not just the piecewise relaxations. A more rigorous approach is using a distance measure between matrices, in this case the proxy measure infidelity, looking at how much the whole density operators differ from the SS.

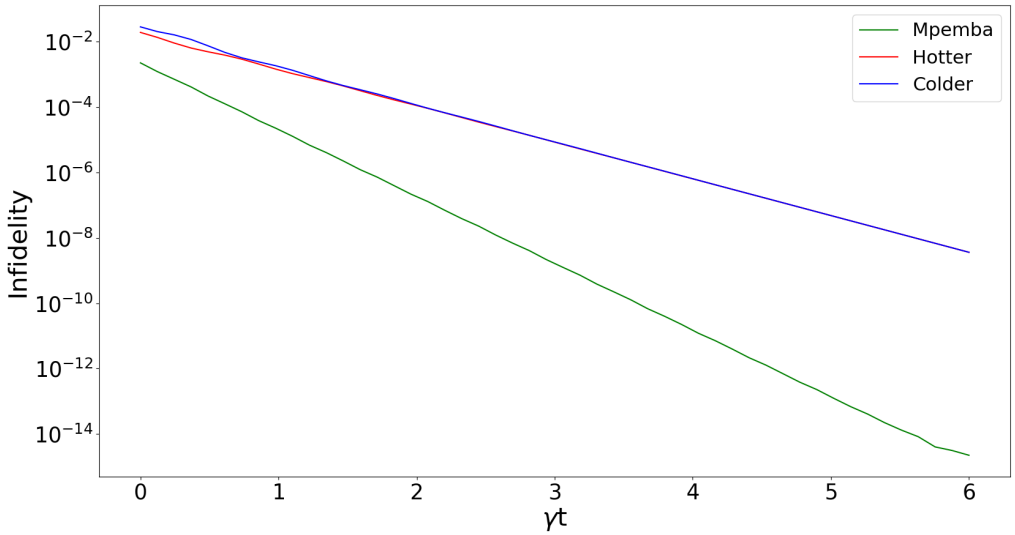

Figure 8: Infidelity $1 - F$ between the known steady state and the time evolved density operator at a given time for different initial temperatures. The infidelity is presented on a log scale.

Looking at the infidelity in Figure 8 the QME becomes visible due to the linear behavior on a log scale. This implies an exponential decay corresponding to only a single decaying mode contributing, which is the case since the decay behavior of the Mpemba state is only governed by $Re(\lambda_3) = Re(\lambda_4)$. For the other states it can be seen that the short time behaviour is not linear, corresponding to multiple modes contributing and then turning linear. The linear part is less steep which shows the SDM dominating in the long time limit, leading to slower relaxation as expected. Further, it is worth noting that the Mpemba state initially has a lower infidelity, so it is inherently closer to the SS, but by eliminating the SDM the relaxation behavior in the long time limit is still accelerated compared to the other states.

Another useful metric to quantify this effect is to investigate how long it takes to relax

the state under varying initial temperatures. To do this, the relaxation time for varying temperature factors is compared at an infidelity threshold, setting the effective SS.

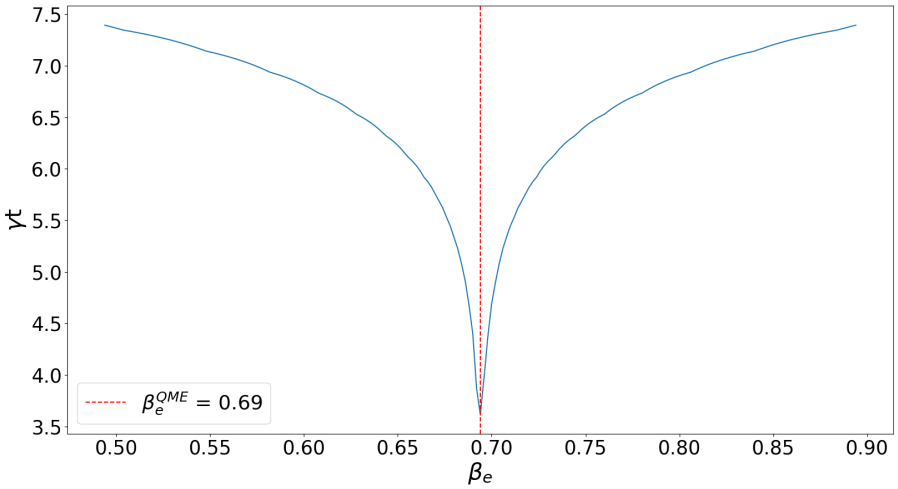

Figure 9: Relaxation time for a range of the temperature factor around the Mpemba state. For a state to reach equilibrium the condition $1 - F = 10^{-10}$ was used. The red dashed line indicates the analytical β_e^{QME} corresponding to the Mpemba state. The little cusps visible are assumed to stem from numerical imprecision due to very small floating point values.

In Figure 9 the Mpemba state is clearly the one with the fastest relaxation time. The surrounding states' relaxation time increases rapidly for both states with a higher and lower temperature factor. There is an asymmetry between the relaxation times in the colder $\beta_e > \beta_e^{QME}$ and the hotter $\beta_e < \beta_e^{QME}$ region, when considering the Mpemba state as the symmetry axis.

5 Discussion

In Figure 6 it can be quite clearly seen that the Mpemba state does correspond to a special geometry as expected by construction. It is visible that the Mpemba state coincides with the equilibrium line of the oscillations in temperature when considering the distance from the SS. This line suggests a very slim temperature region in which this starkly differing behavior occurs, explaining Figure 9, where small deviations from the Mpemba temperature already correspond to a very different relaxation time. The symmetry of the oscillations around the Mpemba state in Figure 6 also poses the question if the QME can be derived from plots such as this one; however, it is not clear how to mathematically describe these oscillations in β_e over time. Overall, due to the fact that both the populations and coherences follow this oscillation behavior and relax towards the Mpemba temperature in the long time limit this thermal state is the fastest decaying one, compared to both hotter and colder states and thereby shows the QME. The oscillatory behavior can also be observed in Figure 7, where the dynamics of different initial states are shown in the complex plane. Here, the oscillations result from the interplay of the real and imaginary part in the coherences, which do not have a classical equivalent and thus justify the quantum mechanical treatment of the ME. While the Mpemba state oscillates, as well as the other states, its oscillations are centered around the SS and deviate much less from the SS value while approaching it as can be seen in Figure 7.

It is worth noting that the plots presented correspond to calculations in the computational basis (as otherwise there would be no coherences) and that the actual thermal state dynamics according to Equation 11 would look different. To avoid this problem the fidelity provides a more certain measure, since it is independent of basis. In Figure 8 it can be seen that the Mpemba state does indeed tend towards stationarity faster. It follows a steeper linear trend which corresponds to the successful elimination of the SDM and the thus accelerated decay. It is worth pointing out that the Mbemba state is the one that starts closest to the SS initially in all different plots. This could indicate that the Mpemba state trivially relaxes faster but the steepness of the infidelity proves a genuine QME.

A limitation of the QME, as presented here, can be said to be the scale at which it takes place. The oscillations in Figure 6 only become visible at very small differences from the steady state, and a large zoom-in is required as seen in Figure 7. Another indicator is Figure 8, in which the accelerated relaxation is visible only for very small infidelity regions, which could prove hard to realize experimentally. Generally, it would be favorable to find the parameter region which exhibits the strongest QME, by finding suitably different eigenvalues. However, as Figure 3 and Figure 4 show, the region with the largest eigenvalue difference

between SDM and other modes (real parts) coincides with the region that approaches the zero temperature limit. Thus there is a tradeoff between how distinct the effect can be, and how cold the initial system has to be.

Furthermore the extent to which this is a purely quantum effect can be discussed. To do this it is worth looking at a coherence free density matrix, which is just governed by a diagonal Hamiltonian and dissipators, similarly to how a classical system would behave. This case can be easily shown in the model by just setting $\omega_y = 0$ and thus getting rid of all off diagonal elements. From Equation 43 it is clear that the Mpemba temperature in the classical limit tends to one. This corresponds to the ground state which is also the SS solution in this case. Since the ground state corresponds to the zero temperature limit it is obvious that this is also the state that decays the fastest. Since this is trivial behavior for a classical system there is no ME to speak of and thus coherences and by extension quantum behavior is essential for the ME in a two level system.

Overall the method of eliminating the SDM to manipulate the relaxation dynamics proved a successful method to explain and show the QME. Further, the phenomenon has an intuitive geometric interpretation in a qubit due to its three dimensional representation as a unit sphere. The plane corresponding to the elimination of the SDM however poses more questions. Since there are many states that lie on this plane, the interpretation of all other states should also be investigated. As temperature was defined via thermal Gibbs states and thus only for states on the axis of the Hamiltonian, the lack of a temperature description for all other states makes characterizing their relaxation behavior in relation to initial temperature difficult. Here an effective temperature could be defined via the trace distance maximization with respect to a thermal state [1].

6 Outlook

This thesis was a brief investigation of the Quantum Mpemba effect in a two dimensional system. It was presented via the elimination of the SDM which also had a convenient geometric interpretation as a plane in the Bloch sphere corresponding to an eliminated SDM and thus accelerated relaxation. Via phase space diagrams of the relaxation, the unique behavior of the Mpemba state compared to other states could be demonstrated. Furthermore, genuine accelerated relaxation in the region close to the SS was presented by using the quantifier infidelity. However, to investigate the QME as a phenomenon in general scenarios in the quantum world many more systems can and should be investigated. An outlook for this system is presented together with prospects for generalizing this to higher dimensions or realizing the QME experimentally.

6.1 This system

The scope of this thesis does not suffice to describe and investigate the system in its entirety. A natural extension would be, as previously mentioned, to examine the eigenvalue behavior compared to the temperature to find the optimal region to observe the QME. Here, the convergence of eigenvalues in relation to a Liouvillian exceptional point could also be taken into consideration, as papers suggest it is connected to the QME [13, 14]. Further the oscillations observed in Figure 6 are left unexplained and can be investigated further. This also leaves open the question whether a mathematical description of these oscillations can be used as an alternative way of obtaining the Mpemba temperature as the SS of these temperature oscillations. Further the system could be investigated with different baths. Currently both baths describe a mixture of dissipation and dephasing as they are not in the diagonal basis of the Hamiltonian. The behavior of a true temperature zero bath could be investigated, corresponding to a σ_- dissipator in the diagonal basis. As the disappearance of ω_y is linked to the disappearance of quantum behavior it is also worth investigating the change of ω_y. Figure 12 in Appendix D highlights such an investigation.

6.2 Higher dimension

A natural candidate for probing the QME in a more general form is to generalize the obtained results to arbitrary dimension size. Since the dimensions of the state space scale as $d^2 - 1$ the geometric interpretation that was given here becomes impossible to visualize and very fast a high dimensional problem that could be more complex to solve. However the QME has been shown to generally exist in quantum systems [10] and more concretely has been

shown in a three level system [13]. Another natural extension to this could also be to look at multipartite systems and see how their coupling to an environment can exhibit Mpemba behavior. Here factors such as entanglement could play a role and make the investigation and outcome be fundamentally different from the two level system.

6.3 Experimental realization

To verify the theoretical predictions and actually put the QME to use it has to be realized experimentally. This comes with many different challenges that need to be taken into account and will also affect the theoretical model since many assumptions and predictions do not hold very well experimentally. Mainly, assumptions such as having the same coupling to σ_z and σ_- are experimentally not really viable since systems, such as trapped ions and superconducting qubits have much shorter decoherence times than relaxation dynamics, leading to different behavior. Furthermore, the accurate preparation of thermal Gibbs states is difficult to achieve experimentally, however progress has been made using variational quantum algorithms, which can be implemented on quantum computers to obtain the desired initial states [21, 22]. The QME has been experimentally shown in different setups [13, 14].

References

[1] F. Ares, P. Calabrese, and S. Murciano, "The quantum mpemba effects," *Nature Reviews Physics*, vol. 7, no. 8, pp. 451–460, 2025. DOI: 10.1038/s42254-025-00838-0.

[2] S. Cecotti, *Statistical Mechanics: A Concise Advanced Textbook*. 2024, ISBN: 978-3-031-67873-8 978-3-031-67874-5. DOI: 10.1007/978-3-031-67874-5.

[3] K. K. Likharev, *Statistical Mechanics: Lecture notes* (2053-2563). 2019, ISBN: 978-0-7503-1416-9. DOI: 10.1088/2053-2563/aaf503.

[4] S. Deffner and S. Campbell, *Quantum thermodynamics: An introduction to the thermodynamics of quantum information*, 2019. arXiv: 1907.01596 [quant-ph].

[5] P. P. Potts, *Quantum thermodynamics*, 2025. arXiv: 2406.19206 [quant-ph].

[6] Aristotle, *Meteorologica*, trans. by H. D. P. Lee. 1952, pp. 79–86.

[7] E. B. Mpemba and D. G. Osborne, "Cool?" *Physics Education*, vol. 4, no. 3, p. 172, 1969. DOI: 10.1088/0031-9120/4/3/312.

[8] M. Jeng, "The mpemba effect: When can hot water freeze faster than cold?" *American Journal of Physics*, vol. 74, no. 6, pp. 514–522, 2006. DOI: 10.1119/1.2186331.

[9] H. C. Burridge and P. F. Linden, "Questioning the Mpemba effect: Hot water does not cool more quickly than cold," *Scientific Reports*, vol. 6, no. 1, p. 37 665, 2016. DOI: 10.1038/srep37665.

[10] M. Moroder, O. Culhane, K. Zawadzki, and J. Goold, "Thermodynamics of the quantum mpemba effect," *Physical Review Letters*, vol. 133, no. 14, 2024. DOI: 10.1103/physrevlett.133.140404.

[11] F. Carollo, A. Lasanta, and I. Lesanovsky, "Exponentially accelerated approach to stationarity in markovian open quantum systems through the mpemba effect," *Physical Review Letters*, vol. 127, no. 6, 2021. DOI: 10.1103/physrevlett.127.060401.

[12] F. Verstraete, M. M. Wolf, and J. I. Cirac, *Quantum computation, quantum state engineering, and quantum phase transitions driven by dissipation*, 2008. arXiv: 0803.1447 [quant-ph].

[13] J. Zhang et al., "Observation of quantum strong mpemba effect," *Nature Communications*, vol. 16, no. 1, 2025. DOI: 10.1038/s41467-024-54303-0.

[14] X. Li, Y. Li, and Y. Yan, *Canonical quantum mpemba effect in a dissipative qubit*, 2025. arXiv: 2511.16996 [quant-ph].

[15] A. Tavakoli and G. Cobucci, "Introduction to quantum information theory," In Press, Oxford University Press, 2026.

[16] G. T. Landi, *Quantum information and quantum noise*, University of Sao Paulo, 2018.

[17] M. A. Nielsen and I. L. Chuang, *Quantum Computation and Quantum Information*. 2000.

[18] D. Manzano, "A short introduction to the lindblad master equation," *AIP Advances*, vol. 10, no. 2, 2020. DOI: 10.1063/1.5115323.

[19] M. Merkli, "Dynamics of open quantum systems ii, markovian approximation," *Quantum*, vol. 6, p. 616, 2022. DOI: 10.22331/q-2022-01-03-616.

[20] F. Campaioli, J. H. Cole, and H. Hapuarachchi, "Quantum master equations: Tips and tricks for quantum optics, quantum computing, and beyond," *PRX Quantum*, vol. 5, no. 2, 2024. DOI: 10.1103/prxquantum.5.020202.

[21] R. Robertson, M. Consiglio, J. Stevens, E. Doucet, T. J. G. Apollaro, and S. Deffner, *Variational gibbs state preparation on trapped-ion devices*, 2026. arXiv: 2603.03801 [quant-ph].

[22] A. N. Chowdhury, G. H. Low, and N. Wiebe, *A variational quantum algorithm for preparing quantum gibbs states*, 2020. arXiv: 2002.00055 [quant-ph].

Appendix A: Finding thermal states with Pauli matrix exponential

For Hamiltonians of the form $\hat{H} = \omega_x\sigma_x + \omega_y\sigma_y + \omega_z\sigma_z$ they can be rewritten as: $\hat{H} = \Omega\hat{n}\cdot\bar{\sigma}$ where $\hat{n} = (\omega_x, \omega_y, \omega_z)/\Omega$ and $\Omega = \sqrt{\omega_x^2 + \omega_y^2 + \omega_z^2}$. Using the anticommutator relationship for pauli matrices: $\{\sigma_i, \sigma_j\} = 2\mathbb{I}\delta_{ij}$ we find that $\hat{H}^2 = \Omega^2\mathbb{I}$. Using the power series of e^x:

$$e^x = \sum_0^\infty \frac{x^n}{n!} \implies e^{-\beta\hat{H}} = \sum_0^\infty \frac{(-\beta\hat{H})^n}{n!} =$$

$$= \sum_0^\infty \frac{(-\beta\hat{H})^{2n}}{(2n)!} + \sum_0^\infty \frac{(-\beta\hat{H})^{2n+1}}{(2n+1)!} = \sum_0^\infty \frac{(-\beta\Omega)^{2n}}{(2n)!}\mathbb{I} + \sum_0^\infty \frac{(-\beta\Omega)^{2n}(-\beta\hat{H})}{(2n+1)!}\mathbb{I} =$$

$$= \cosh(\beta\Omega)\mathbb{I} + \sum_0^\infty \frac{(-\beta\Omega)^{2n+1}\hat{n}\cdot\bar{\sigma}}{(2n+1)!} = \cosh(\beta\Omega)\mathbb{I} - \sinh(\beta\Omega)\frac{\hat{H}}{\Omega}$$

Since $\cosh(x) = \cosh(-x)$ and $-\sinh(x) = \sinh(-x)$. For $\hat{H} = \omega_y\sigma_y + \omega_z\sigma_z$ we have $\mathrm{tr}\Big(\exp\Big(-\beta\hat{H}\Big)\Big) = 2\cosh(\beta\Omega)\mathbb{I}$ So

$$\rho_{th} = \frac{1}{2}(\mathbb{I} - \tanh(\beta\Omega)\frac{\hat{H}}{\Omega})$$

Appendix B: Properties of the Eigenvalues

As already mentioned the eigenvalues can be found using Cardano's formula for the solutions to a depressed cubic. The polynomial

$$(80\omega_y^2\gamma + 32\omega_z^2\gamma + 50\gamma^3 + (16\omega_y^2 + 16\omega_z^2 + 45\gamma^2)\lambda + 12\gamma\lambda^2 + \lambda^3),$$

can be written as $a\lambda^3 + b\lambda^2 + c\lambda + d$, where $a = 1$, $b = 12\gamma$, $c = (16\omega_y^2 + 16\omega_z^2 + 45\gamma^2)$ and $d = 80\omega_y^2\gamma + 32\omega_z^2\gamma + 50\gamma^3$. The corresponding depressed cubic can be found by substituting $w = \lambda + \frac{b}{3a} = \lambda + 4\gamma$. With this the depressed cubic, that can be solved according to the solutions seen in Equation 33 is of the form

$$w^3 + pw + q = 0.$$

Here, p and q are found by substituting $\lambda = w - 4\gamma$ into the original polynomial. This gives

$$d + c(w - 4\gamma) + 12\gamma(w^2 - 8w\gamma + 16\gamma^2) + w^3 - 12\gamma w^2 + 48w\gamma^2 - 64\gamma^3$$

. After rearranging and simplifying this gives

$$(d - 4\gamma c + 128\gamma^3) + (c - 48\gamma^2)w + w^3.$$

This leads to the final expressions of p and q to be found in the main thesis. Further from this the analytical discriminant can also be computed to be

$$\Delta = \frac{1}{27}\left(16\left(\omega_y^2 + \omega_z^2\right) - 3\gamma^2\right)^3 + \gamma^2\left(\gamma^2 - 8\omega_y^2 + 16\omega_z^2\right)^2$$

Further the inequality in Equation 36 should be derived. To have a nondegenerate SDM the Real part of the SDM should be greater than of all other decaying modes. Since $\Delta = 0$ gives degeneracies and three real solutions are not considered it is needed that $\Delta > 0$. How this is given in the parameter region chosen can be seen in Figure 10. Further for this to hold

$$Re(\lambda_2) > Re(\lambda_{3,4}) \implies -4\gamma + w_0 > -4\gamma - \frac{1}{2}w_0 \implies w_0 > -\frac{1}{2}w_0.$$

Here w_0 is the solution of the depressed cubic corresponding to λ_2 and is real due to the positive discriminant. The real parts of the other eigenvalues reduce to the same root up to a factor which gives the inequality. From this it is trivial that the inequality above holds for all positive w_0. Which is the inequality in Equation 36. This can be plotted to determine a constraint on the viable parameter region in Figure 11.

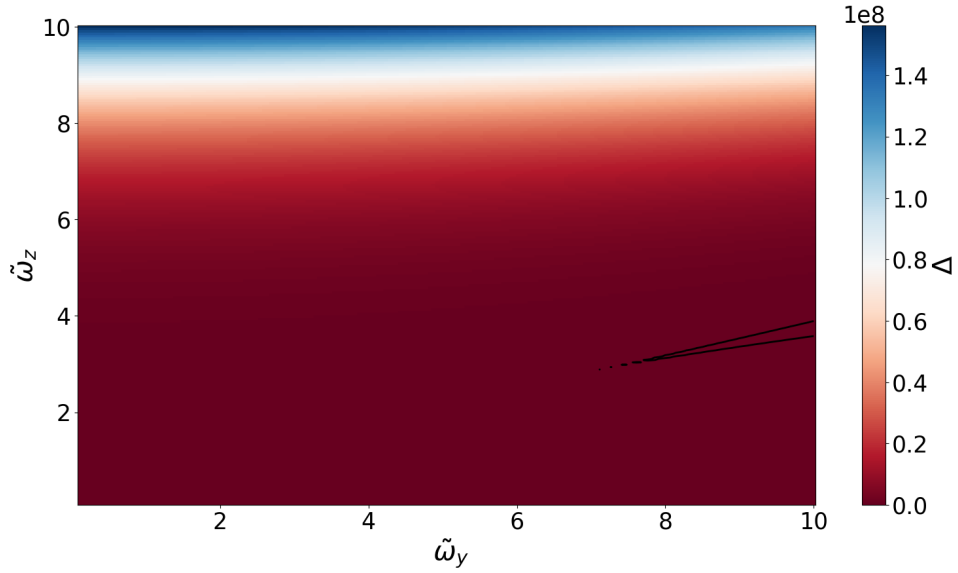

Figure 10: Discriminant behavior. The discriminant is mainly positive so not a constriction on the parameters, except for a small region, indicated by the black line, which however is eligible due to other constraints anyways.

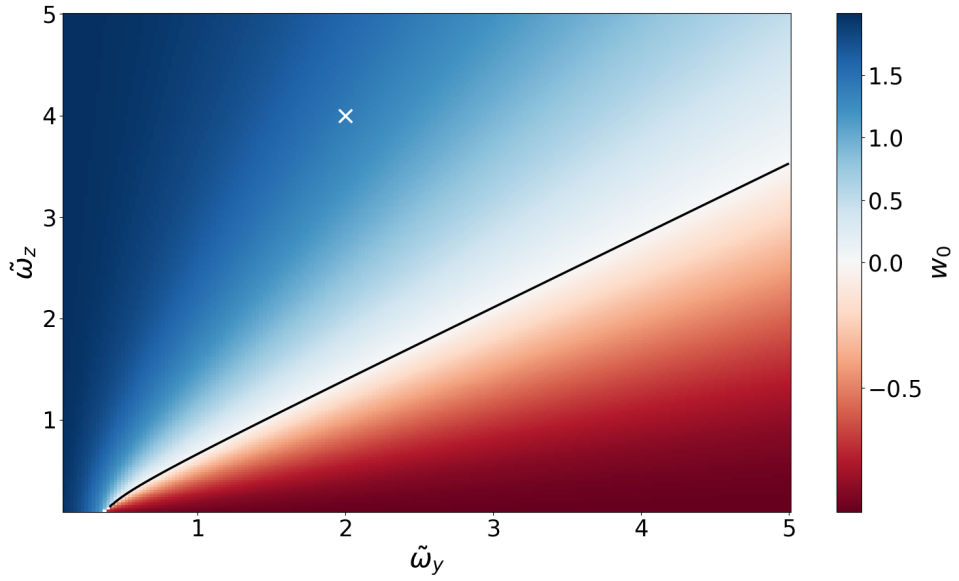

Figure 11: Contour plot of the parameter region with the Black line indicating the sign of w_0 above the line $w_0 > 0$ corresponding to a viable non-degenerate SDM.

Appendix C: Extended visualization of relaxation behavior

In the following the snapshots for the full time evolution from $\gamma t = 0$ to $\gamma t = 6$ are presented, this corresponds to the same zooming-in process that can be seen in Figure 7 but here all time steps are presented.

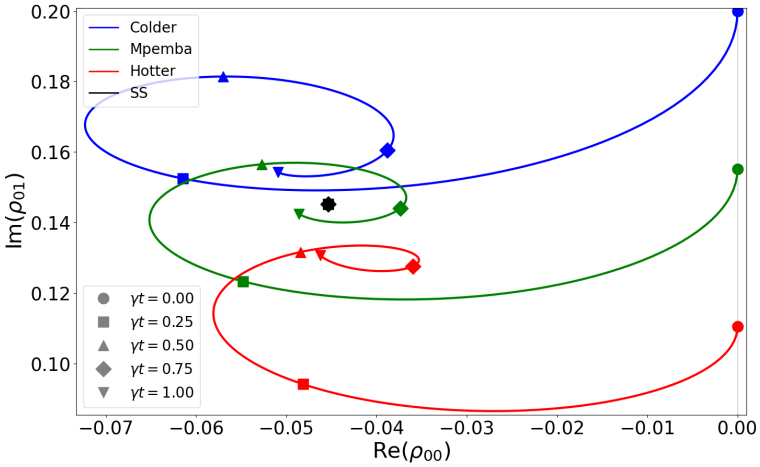

$\gamma t = 0$ to $\gamma t = 1$

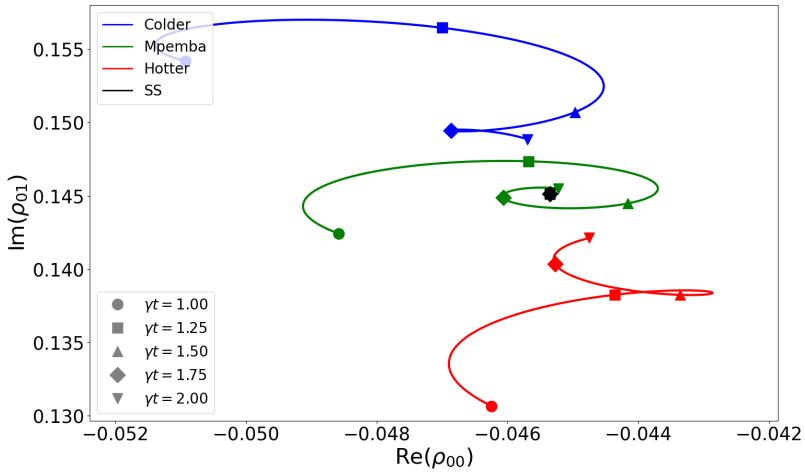

$\gamma t = 1$ to $\gamma t = 2$

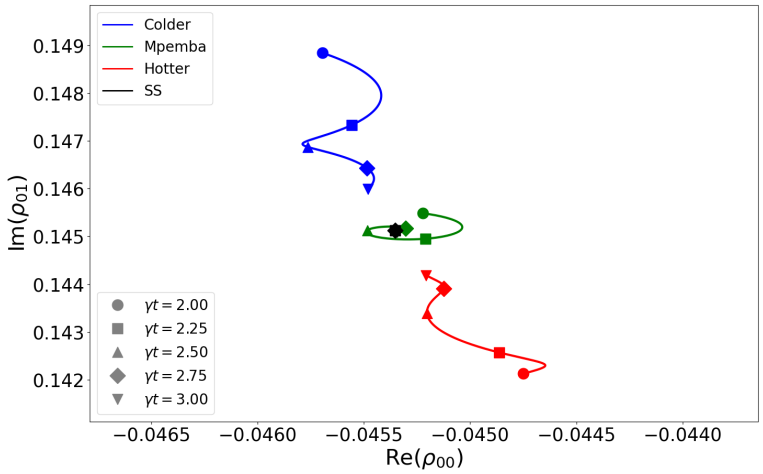

$\gamma t = 2$ to $\gamma t = 3$

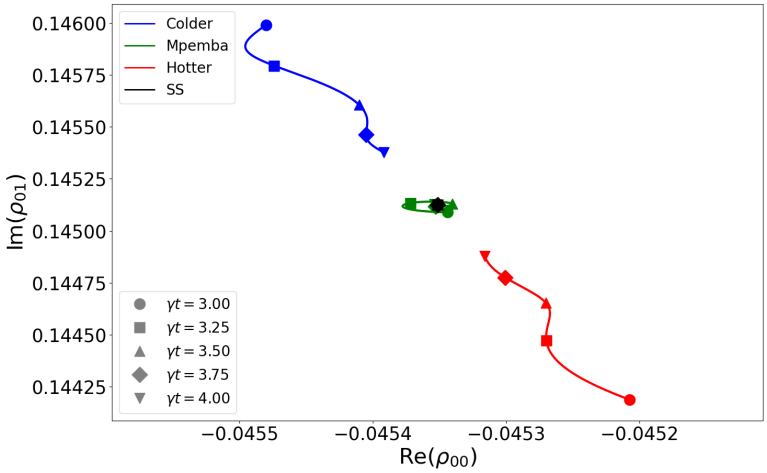

$\gamma t = 3$ to $\gamma t = 4$

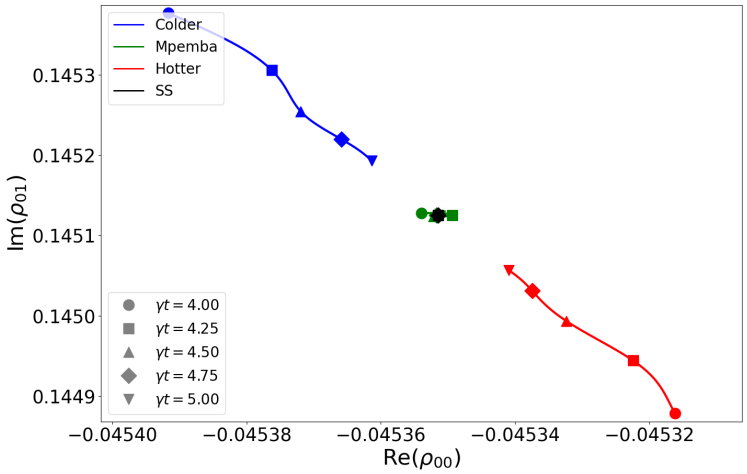

$\gamma t = 4$ to $\gamma t = 5$

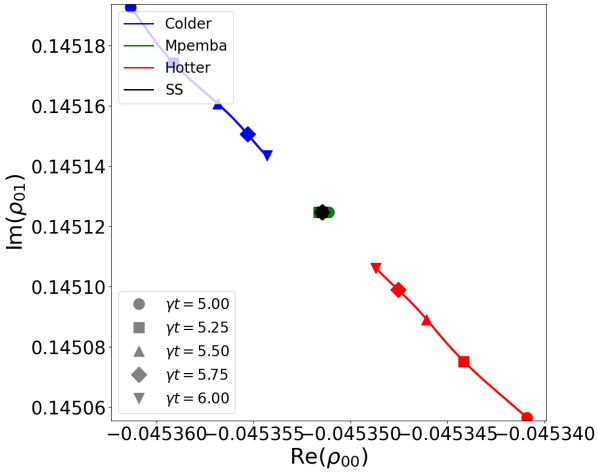

$\gamma t = 5$ to $\gamma t = 6$

Appendix D: Sweeping ω_y

From Equation 12 it is known that the appearance of coherences in the computational basis stem only from the ω_y contribution. Thus it is worth investigating the behavior of the Mpemba temperature with respect to ω_y. An interesting correlation to the derivative of the deviation from the Z axis could also be established. These findings are presented in Figure 12.

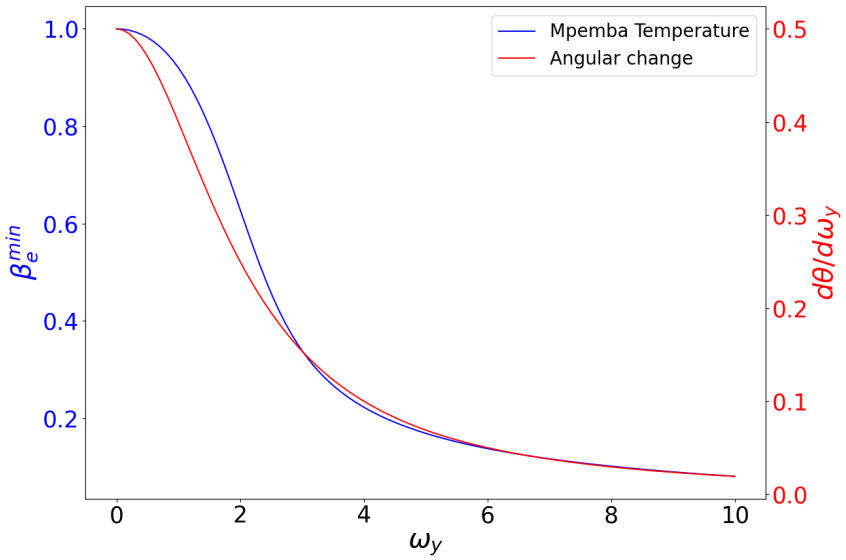

Figure 12: Change in Mpemba temperature (left) vs. ω_y, corresponding to σ_y contribution in the Hamiltonian in Blue. Angular rate of change with respect to ω_y (right) vs. ω_y in Red

Since this is an interesting result but not the focus of this thesis and cannot be properly explained in the scope of this thesis it is only presented here, maybe as something to investigate in the future.